Invesigation of the Anisotropic Nature of Laser Generated Ultrasound in Zinc and Unidirectional Carbon Epoxy Composites

David H. Hurley
James B. Spicer
James W. Wagner
Todd W. Murray

Johns Hopkins University
Dept of Materials Science and Engineering
102 Maryland Hall
Baltimore, MD 21218

ABSTRACT

Laser generated ultrasound in carbon epoxy composites provides an ultrasonic signature which is difficult to interpret owing to the elastic anisotropic and inhomogeneous nature of these materials. In the present work, a line source representation of laser-generated ultrasound in materials exhibiting transverse isotropy is presented. The bounding plane of the half space is assumed to be the plane of isotropy. Neglecting thermal diffusion, it is shown that in the limit of strong optical absorption, the buried line source is equivalent to applying a shear stress dipole at the bounding surface. A formal solution is found using double (Fourier-Laplace) transforms. The Cagniard-de Hoop technique is used to analytically invert the transform for the epicentral case as well as the surface wave case. A solution for a sub-surface source is obtained numerically.

Experimental validation of the theory is performed using single crystal zinc and a unidirectional carbon epoxy sample with the plane of isotropy perpendicular to the fiber direction. For zinc, the experimentally obtained epicentral and surface wave displacements agree well with theoretical predictions. The carbon epoxy sample exhibits homogeneous behavior when the wave vector is perpendicular to the fiber direction. When the wave vector is aligned with the fiber direction, the wave form appears to be influenced by the inhomogeneous nature of the composite.

INTRODUCTION

Laser generated ultrasound has been used to determine material properties and to characterize material defects [1-3]. To a large extent, the success of laser ultrasonics has been the researcher's ability to correctly predict the temporal evolution of the displacement waveform resulting from pulsed laser irradiation. Theories that assume isotropic elastic properties work well for crystalline materials that have randomly oriented grains with grain sizes that are small compared to the wavelength of the interrogating ultrasonic wave [4-5]. For single crystal samples or carbon epoxy composites, the elastic anisotropic nature must be taken into account. A number of researchers have shown that the behavior of single crystal materials in the presence of an ultrasonic disturbance differ markedly from their isotropic counterparts [6-13]. Mourad *et al.* [6] used the Cagniard-de Hoop method [14] to numerically obtain the solutions to Lamb's [15] problem in an anisotropic half-space. In their paper, Mourad *et al*. assumed that the laser source could be modeled as a shear stress dipole applied at the bounding surface. In addition, Weaver *et al.* [7] have studied the elastodynamic response of a thick transversely isotropic plate to a normal point source applied at the bounding surface. Of particular interest is the work by Payton [13], who has treated a general class of problems for crystals that exhibit transverse isotropy. Payton [13] gives an explicit set of conditions, related to the elastic parameters of the material, that predict the existence of inflection points on the slowness curve.

In this paper a set of boundary conditions which are equivalent to a thermoelastic point-source in a strongly absorbing material are developed. Analytical expressions for the surface wave and for waves traveling along the symmetry axis are given for materials that exhibit transverse isotropy. These analytical

expressions are compared with experimental waveforms generated in a sample of single crystal zinc and in a sample of unidirectional carbon fiber epoxy composite. In addition, inhomogeniety due to variations in optical properties is considered by modeling a sub-surface source. The epicentral displacement resulting from a buried source is obtained numerically.

THEORY

EQUIVALENT BOUNDARY CONDITIONS

The first work to give a quantitative scientific basis to pulsed laser ultrasonics was that of Scruby *et al.* [1]. In this work, the thermoelastic source for strongly absorbing materials, such as metals, was reported to be equivalent to a shear stress dipole applied at the bounding surface. Later, Rose [4] gave a systematic derivation for a point-source representation for laser generated ultrasound. In this presentation, Rose showed that by neglecting the effects of heat conduction, the laser source can be approximated by a surface center of expansion (SCOE). In addition, Rose demonstrated that the SCOE is equivalent to the shear stress dipole source proposed by Scruby *et al.* [1].

In his development , Rose considers the center of expansion to be buried some distance below the free surface in order to correctly evaluate the elastic boundary conditions. For strongly absorbing materials, the source is brought to the surface where it is shown to be equivalent to a shear stress dipole applied at the bounding surface. For an anisotropic half space, the procedure presented by Rose is long and cumbersome owing to the fact that the shear and longitudinal deformations cannot be uncoupled.

As an alternative, a method of images is used to aid in the development of an equivalent set of boundary conditions for an anisotropic half-space, Nowacki [16]. To understand the method of images consider an infinite, transversely isotropic elastic medium. The axis of symmetry is parallel to the x_3 axis. The medium is subjected to a line center of expansion and a line center of contraction as shown in Fig 1. The plane of separation, formed by the x_2 and x_3 coordinate axes, is midway between the two sources and is perpendicular to the line joining the two sources. This type of arrangement will result in a nonzero shear stress state, and a zero normal stress state at the plane of separation. If at the separation plane, a shear stress of opposite sign to the shear stress resulting from the source sink combination is applied, a stress free state will be obtained at the separation plane. The separation plane can now be identified with the bounding surface of an elastic half space. Upon bringing the source and sink to the boundary, the equivalent stress boundary conditions become

$$\left(\sigma_{23}\right)\Big|_{x_3=0} = \tilde{F}\,\delta'(x_2)H(\tau), \quad \left(\sigma_{33}\right)\Big|_{x_3=0} = 0$$
$$\tilde{F} = (F_3 + F_2\alpha - F_3\kappa). \tag{1}$$

where $\delta'(x_3)$ is the spatial derivative of the Dirac delta function and $H(\tau)$ represent a unit step function. F_2, F_3, α, and κ are functions of the elastic stiffnesses and the thermal constants and are represented as follows:

$$\alpha = \frac{c_{33}}{c_{44}}, \beta = \frac{c_{11}}{c_{44}}, \tau = t\left(\frac{c_{44}}{\rho}\right)^{1/2}, \kappa = (1+\alpha\beta-\gamma)^{1/2},$$
$$\gamma = 1+\alpha\beta-\left(\frac{c_{13}}{c_{44}}+1\right)^2, F_2 = \frac{B_{22}T_o}{C_{44}}, F_3 = \frac{B_{33}T_o}{C_{44}} \tag{2}$$

where B_{ij} are the components of the thermal expansion tensor, T_o is the ambient temperature and C_{ij} are the components of the stiffness tensor.

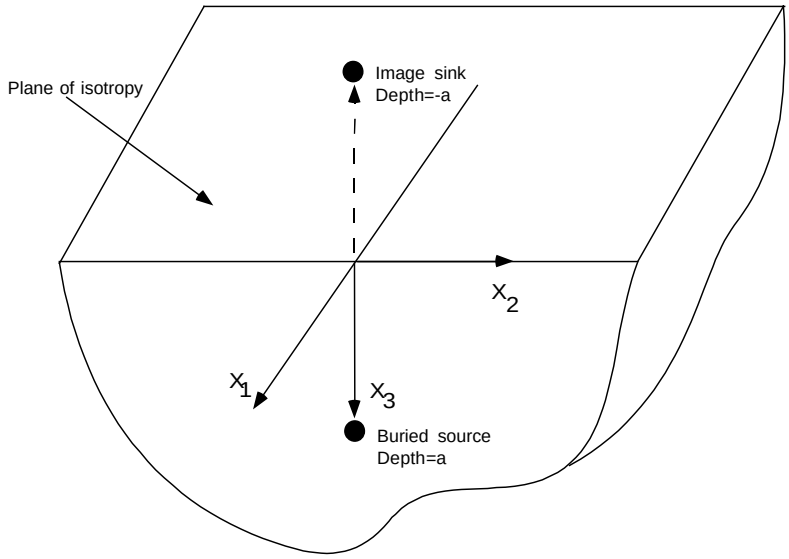

Fig 1. Problem geometry with source and sink locations.

HALF SPACE SUBJECTED TO SHEAR STRESS DIPOLE

A line source representation for laser generated ultrasound is presented using the equivalent boundary conditions listed in Eq. 1. The equations of motion are written as:

$$\begin{aligned} \beta u_{2,22} + u_{2,33} - u_{2,\tau\tau} + \kappa u_{3,23} &= 0 \\ \kappa u_{2,23} + u_{3,22} + \alpha u_{3,33} - u_{3,\tau\tau} &= 0 \end{aligned} \tag{3}$$

The solution technique proceeds by applying Fourier and Laplace transforms to eliminate dependence on the spatial and temporal variables, respectively, and then inverting the transformed equations using the Cagniard-Pekeris [14-17] inversion technique. The general solution is of the form

$$\begin{aligned} \bar{u}_2(\eta, x_3, s) &= A_1 e^{ik_1 x_3} + A_2 e^{ik_3 x_3}, \\ \bar{u}_3(\eta, x_3, s) &= A_3 e^{ik_1 x_3} + A_4 e^{ik_3 x_3}. \end{aligned} \tag{4}$$

Where $A_{1\text{-}4}$ are obtained by satisfying the equations of motion and the boundary conditions, and $k_{1/3}$ are the physical roots to the slowness curve. Next, the following substitution is made so as to facilitate the Cagniard-Pekeris inversion:

$$k = s\bar{\zeta}, \eta = s\omega. \tag{5}$$

The physical roots to the slowness curve are written as:

$$
\begin{aligned}
i\bar{\zeta}_1(\omega) &= \left[\frac{((\alpha+1)+\gamma\omega^2)+\sqrt{\phi(\omega)}}{2\alpha}\right]^{1/2} = -\zeta_1(\omega)\ , \\
i\bar{\zeta}_3(\omega) &= \left[\frac{((\alpha+1)s+\gamma\omega^2)-\sqrt{\phi(\omega)}}{2\alpha}\right]^{1/2} = -\zeta_3(\omega), \\
\phi(\omega) &= \left[\gamma\omega^2+(\alpha+1)\right]^2 - 4\alpha\left[\beta\omega^4+(\beta+1)\omega^2+1\right].
\end{aligned} \tag{6}
$$

Borrowing notation used by Payton [13], the behavior along the symmetry axis of crystals that exhibit elastic transverse isotropy can be divided into three categories according to the nature of their anisotropy:

$$
\begin{aligned}
&\text{(i)} && (\alpha+\beta)<\gamma<(1+\alpha\beta), \\
&\text{(ii)} && (\beta+1)<\gamma<(\alpha+\beta) \ \text{ and } \ (\gamma^2-4\alpha\beta)<0, \\
&\text{(iii)} && \gamma<(\beta+1) \ \text{ and } \ (\gamma^2-4\alpha\beta)<0 \ \text{ also } \ \beta>\alpha
\end{aligned} \tag{7}
$$

For crystals belonging to class (i), the roots of the slowness equation are purely imaginary, while crystals belonging to classes (ii) and (iii) have complex roots and the wave-front curves for these crystals have cuspidal triangles. For class (iii) crystals, the triangluar portion of the wave-front is centered on the symmetry axis.

SOLUTIONS ALONG THE BOUNDING SURFACE

For solutions along the bounding surface, the Fourier inversion path is along the real ω axis, and the Cagniard path is along the imaginary ω axis. Presently, only the inversion of $\bar{u}_3$ is being considered. Since $\bar{u}_3$ is an even function of $\sqrt{\phi(\omega)}$, the solution technique is the same regardless of the crystal class. The analytical expression for the solution can be written as:

$$
u_3(x_2,0,\tau) = \tilde{F}\left\{\frac{\bar{\psi}_r}{|x_2|}\delta(T_2-\omega_r)+\frac{1}{|x_2|\pi}g(T_2)\left[H(T_2-1/\sqrt{\beta})-H(T_2-1)\right]\right\}, \tag{8}
$$

where

$$
g(T_2) = \frac{\tilde{F}T_2{}^2\alpha\zeta_1\zeta_3\left[(1-\kappa)(1-2T_2{}^2)-(\alpha-\gamma T_2{}^2)\right]}{\left[-2(1-\kappa)T_2{}^2+\gamma T_2{}^2-\alpha\right]^2(1-T_2{}^2)+\alpha(\beta T_2{}^2-1)}, \quad T_2=\frac{\tau}{|x_2|}. \tag{9}
$$

SOLUTIONS ALONG EPICENTRAL AXIS

Another class of solutions that can easily be inverted using the Cagniard-Pekeris technique is that for displacements along the epicentral axis. The Cagniard path depends on the category of crystal being investigated. For materials belonging to class (i), the Cagniard path is along the real ω axis. For class (ii) and (iii) materials, the Cagniard path is off the real ω axis. The analytical expression for the epicentral displacement for class one crystals is given by,

$$
u_3(0,x_3,t) = \frac{\tilde{F}}{\pi}\mathrm{Re}\left\{\left(\bar{A}_3\frac{\partial\varpi_1}{\partial\tau}\right)H(T_3-1)+\left(\bar{A}_3\frac{\partial\varpi_1}{\partial\tau}\right)H(T_3-1/\sqrt{\alpha})\right\}, \quad T_3=\frac{\tau}{x_3}, \tag{10}
$$

where $\overline{A}_{3/4}$ are obtained by satisfying the boundary. For class (ii) and class (iii) materials, the Cagniard path no longer lies on the real ϖ axis. Applying the Cagniard technique to class (ii) and class (iii) materials gives

$$u(0,x_3,\tau) = \tilde{F}J(T_3) = \frac{\tilde{F}}{\pi}\left\{\begin{array}{l} \overline{A}_4\left(\frac{\partial\varpi_{\bar{1}\to\bar{2}}}{\partial\tau}\right)\left\{H(T_3-T_e)-H(T_3-1)\right\}+ \\ \overline{A}_3\left(\frac{\partial\varpi_{\bar{2}\to\bar{3}}}{\partial\tau}\right)\left\{H(T_3-1/\sqrt{\alpha})-H(T_3-T_e)\right\}+\overline{A}_4\left(\frac{\partial\varpi_{\bar{3}\to\bar{4}}}{\partial\tau}\right)\left\{H(T_3-T_+)\right\} \end{array}\right\} \quad (11)$$

SOLUTIONS ALONG EPICENTRAL AXIS DUE TO A BURIED LINE SOURCE

Inhomogeniety due to variations in optical properties is considered by modeling a sub-surface source. Due to length requirements, only a brief summery of the solution technique for a buried line source in a transversely isotropic half-space is given. Since the source is buried, the expression for the Cagniard path must be obtained numerically. If Beryl is used as an example, the numerical solution can be represented by the following expression:

$$u(0,x_3,\tau) = DL + DS + RL + RS + ML + MS, \quad (12)$$

where the expressions DL, DS, RL, RS, ML, MS represent the direct longitudinal, the direct shear, the reflected longitudinal, the reflected shear, the mode converted longitudinal and the mode converted shear wave respectively. It should be noted that for a buried line source in a transversly isotropic material, there are six wave arrivals while, for isotropic materials, there are only three wave arrivals. The presence of six waves is due to the thermoelastic production of shear waves. It is commonly known that a thermoelastic source in an unbounded isotropic material does not produce shear waves. The production of shear waves in an anisotropic material is a result elastic and thermal anisotropy.

EXPERIMENT

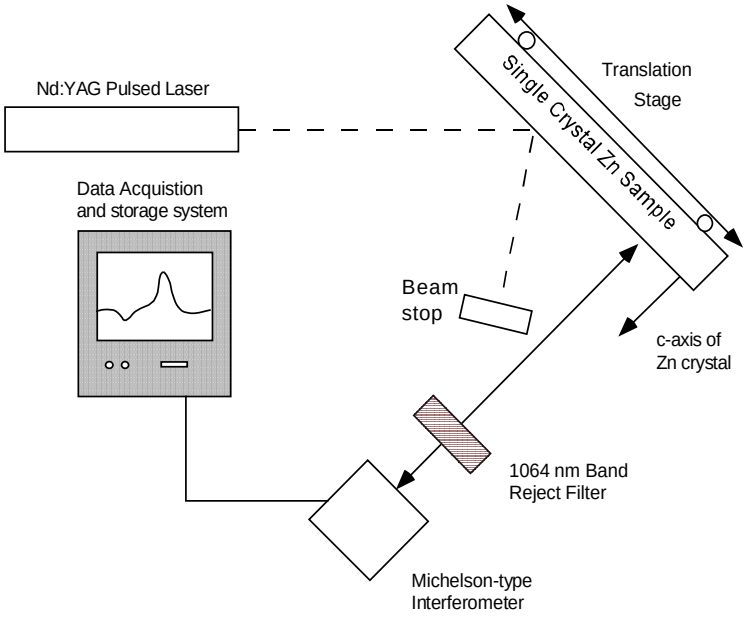

Fig. 2. Experimental setup. A Nd:YAG laser is used to generated the ultrasound and a Michelson interferometer is used to detect the ultrasound.

The experimental setup used to generate surface waves was shown in Fig. 2. The generation of the ultrasonic disturbance was accomplished by irradiating the sample with a pulsed Nd:YAG laser operating at 1.064 μm, with a Gaussian transverse spatial profile.

A cylindrical lens was used to focus the generation beam to a line, whose full width half maximun (FWHM) was about 2 cm. Care was taken so as not to ablate the sample surface. The pulse duration was 10 ns with a typical pulse energy 20 mJ . The ultrasonic disturbance was detected on the same side as the generation beam with a Michelson-type interferometer operating at 632.8 nm. The detection bandwidth of the interferometer was estimated to be in excess of 50 MHz.. The voltage signals from the interferometer were recorded using a LeCroy 9354m digital oscilloscope operating at 500 Msamples/s. The experimental setup for detection of epicentral waves was similar to the one shown in Fig. 2, except that the generation and detection points were on opposite sides of the sample.

RESULTS AND DISCUSSION

In Figs. 3 and 4, a comparison between theorry and experiment for same side detection is presented for zinc and graphte epoxy respectively. In Figs 3 and 4, the theoretical results are convolved with a Gaussian function (FWHM 400 ns) in order to mimic the finite generation pulse duration and the transit time of the ultrasonic disturbance across the detection spot. In Fig. 3, the first disturbance turns on and off at times corresponding to the arrival of the longitudinal wave and shear wave respectively. The largest disturbance corresponds to the Rayleigh pole and is in the form of a traveling delta function. In Fig. 4, the experimental and theoretical results for a sample of unidirectional graphite epoxy are presented. The fiber direction is perpendicular to the sample surface and hence the bounding surface is a plane of isotropy. The overall character is similar to that of the zinc sample but the pulse appears to be temporally broadened. The pulse broadening or frequency dependent attenuation in Fig. 4 is most likely due to scattering effects or viscoelastic effects.

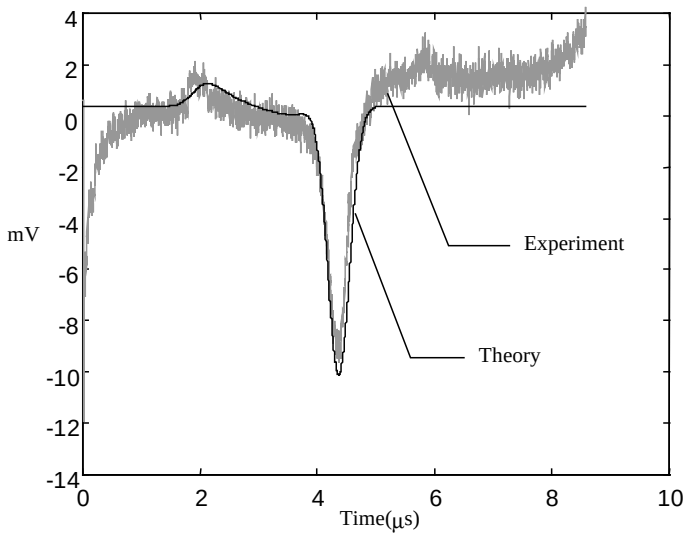

Fig 3. Comparison between experiment and theory for surface waves generated with a line source in zinc.

In Fig. 5, an epicentral wave-form is shown for a sample of unidirectional graphite epoxy. The fiber direction is parallel to the sample's surface and also parallel to the line source. In order to account for the finite generation pulse duration, the theoretical result was convolved with a Gaussian pulse with a FWHM of 20 ns. The sample of graphite epxoy for this type of configuration should appear elastically isotropic. Figure 5 shows a close agreement between theory and experiment, reaffirming the claim of transverse isotropy.

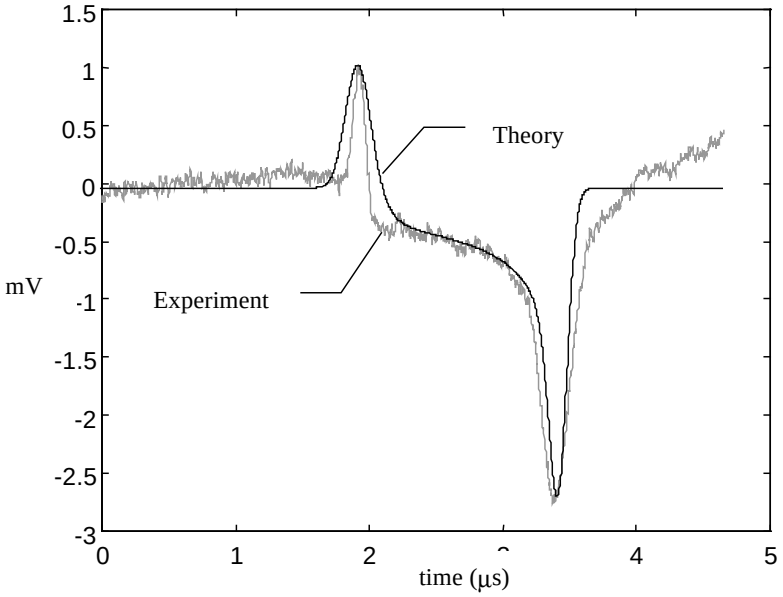

Fig. 4. Comparison between experiment and theory for surface waves generated with a line source in graphite epoxy

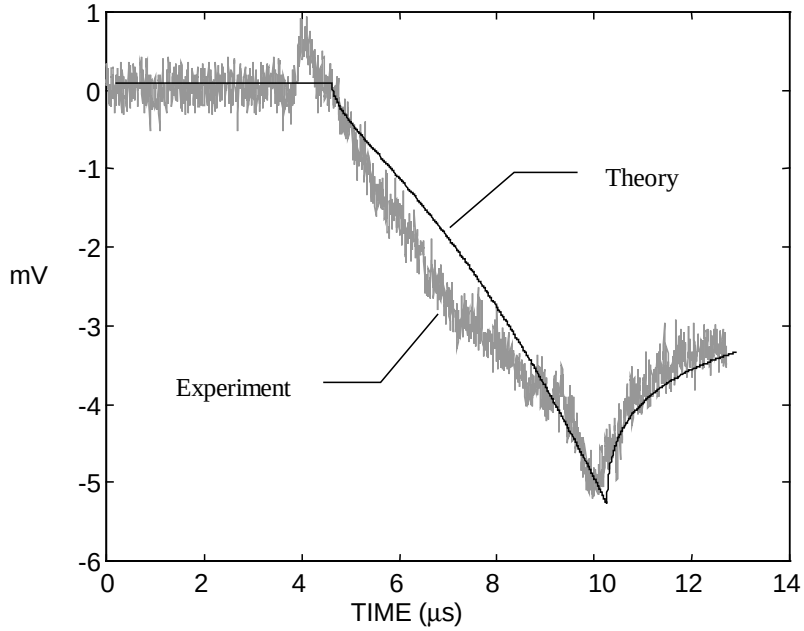

Fig. 5. Epicentral waveform in graphite epoxy. The fibers are parallel to the surface and the line source. This type of arrangement leads to isotropic behavior.

A comparison between the theoretical and experimental epicentral displacements resulting from a laser line source in zinc is shown in Fig. 6. The crystallographic c axis was perpendicular to the bounding plane. Again, the theoretical result was convolved with a Gaussian pulse with a FWHM of 20 ns. Zinc is a class three crystal and as a result, the displacement character differs markedly form its isotropic counterpart. In a fashion similar to that of the surface wave case, the first disturbance turns on and off at times

corresponding to the arrival of the longitudinal wave, t_l, and shear wave, t_s, respectively. After t_s, the Greens tensor is identically zero until the arrival of the majority of the acoustic energy at t_+. The disturbance that arrives a t_+ results from a reciprocal square root singularity displauing behavior not found in isotropic materials or class (i) materials.

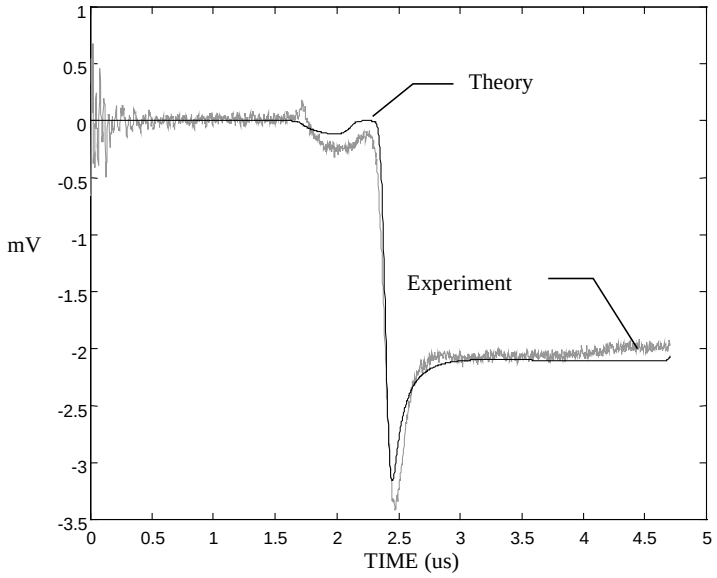

Fig. 6. Experiment and theory for epicentral waves generated with a line soruce in zinc.

Figure 7 compares theoretical results for a surface line source and a buried line source in the mineral Beryl. For this case, the plane of transverse isotropy is the bounding plane and the detection location is located along the symmetry axis. The ratio of the sample thickness to the source depth, X_a, is 5000. For Beryl, the cuspidal triangular portion of the wave-front does not intersect the symmetry axis. As a result, the wave form exhibits characteristics similar to its isotropic counterpart. The waveform for the buried source shows a precursor spike that is a result of bulk waves reflecting off the stress free boundary. Since X_a is large, it is impossible to discern 6 distinct wave arrivals.

Epicentral wave forms resulting from a point source in graphite epoxy are shown in Fig. 8. The beam diameter used to generated these wave forms was 0.4mm and 1 mm. The fiber direction is perpendicular to the bounding surface and hence the bounding surface is the plane of isotropy. The wave form generated by the smaller beam diameter exhibits frequency dependent dispersion which may be a result of the heterogeneous character of the graphite epoxy.

CONCLUSION

Analytical results for the displacement resulting from a laser line source was obtained for materials that exhibit transverse isotropy. The theoretical expressions for the surface and epicentral cases were compared to the experimental results for a sample of single crystal zinc. For both cases, the theory and the experiment showed close agreement. In addition, experimental results for unidirectional graphite epoxy were obtained. The carbon epoxy sample exhibited homogeneous behavior when the wave vector is perpendicular to the fiber direction. When the wave vector is aligned with the fiber direction, the wave form appears to be influenced by the inhomogeneous nature of the composite.

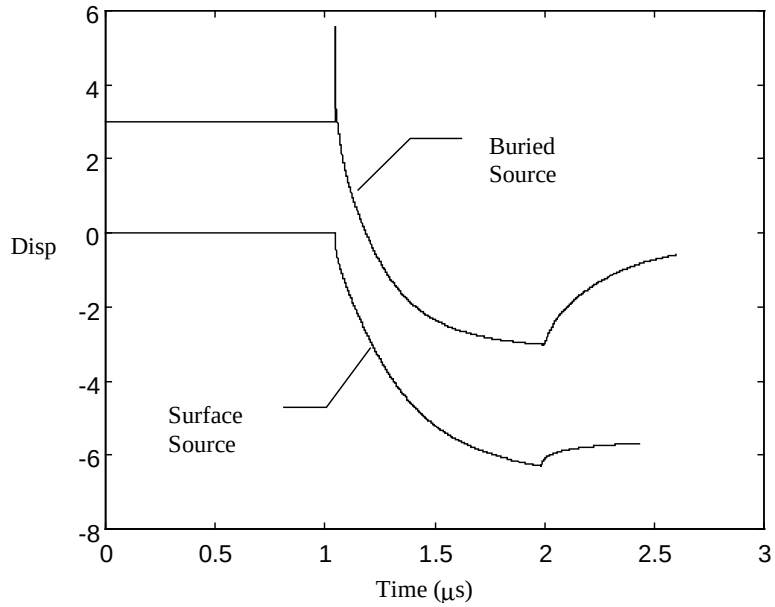

Fig. 7. Comparision between theoretical wave forms generated with a surface source and a buried source.

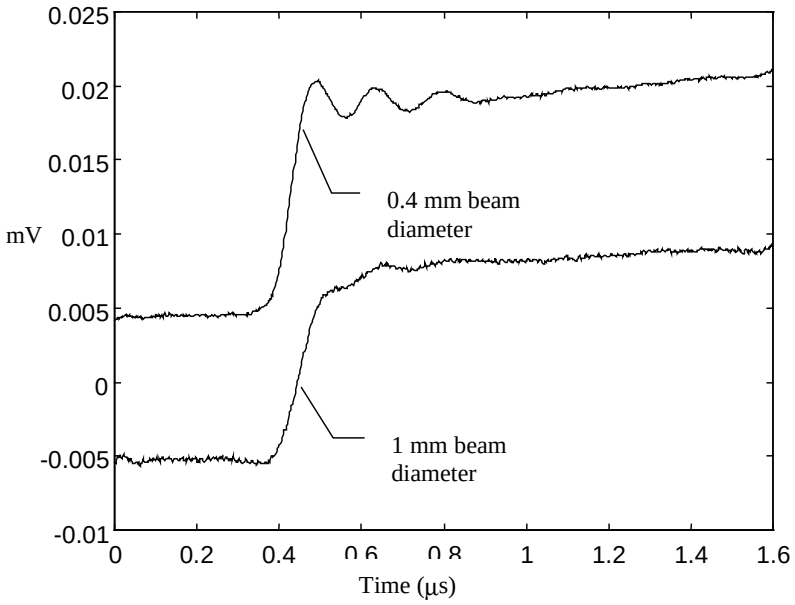

Fig. 8. Showing the effect of generation spot size on the epicentral displacement in graphite epoxy.

REFERENCES

1. Scruby, C. B., Dewhurst, R. J., Hutchins, D. A., Palmer, S.B., Quantitative Studies of Thermally Generated Elastic Waves in Laser-Irradiated Metals, *Journal of Applied Physics* (1980) **51** 6210-6216.
2. Scruby, C. B., Smith, R. L., Moss, B. C., NDT Int (1986) **19**, 307.
3. Telschow, K., *Review of Progress in Quantitative Nondestructive Evaluation*, (Plenum, New York, 1988) Vol. 7b, p.1211.
4. Rose, L. R. F., Point Source Representation for Laser Generated Ultrasound, *Journal*

of the Acoustical Society of Americal (1984) **73** 723.
5. Telschow, K., Conant, R., Optical and Thermal Parameter Effects on Laser Generated Ultrasound, *Journal of the Acoustical Society of America* (1990) **88**, 1494-1502.
6. Mourad, A., Deschamps, M., Castangnède, B., Acoustic Waves Generated by a Transient Line Source in an Anisotropic Half-Space, *Acustica* (1996) **82** 839-851.
7. Weaver, R. L., Sachse, W., Kwang, Y.K., Transient Elastic Waves in a Transversely Isotropic Plate, *J Applied Mech* (1996) **63** 337-346.
8. Royer, D., Dieulesaint, E., Rayleigh Wave Velocity and Displacement in Orthorhombic, Tetragonal, Hexagonal, and Cubic Crystals, *Journal of the Acoustical Society of America* (1984) **76** 1438-1444.
9. Kraut, E. A. *Rev. Geophys* (1963) **1** 401.
10. Burridge, R., Lamb's Problem for an Anisotropic Half-Space, *Quarterly Journal of Mechanics and Applied Mathematics*, **24**, 81-98, (1970).
11. Willis, J. R., and Bedding, R. J., Arrivals Associated with a Class of Self-Similar Problems in Elastodynamics, *Mathematical Proceedings of the Cambridge Philosophical Society*, **77**, 591-607, (1975).
12. Musgrave, M. J. P. *Crystal Acoustics*, Holden-Day, Inc., San Francisco (1970).

13. R.G. Payton, *Elastic Wave Propagation in Transversely Isotropic Media*, Martinus Nijhoff Publisher, The Hague (1983).
14. Cagniard, L., *Reflection and Refraction of Prog. Seismic Waves* New York, McGraw-Hill (1962).
15. Lamb, H. *Phil. Trans. Roy. Soc.* (1904) A203 **1.**
16. Nowacki, W. *Dynamic Problems of Thermoelasticity*, Polish Scientific Publishers, Warszawa (1975).
17. Pekeris, C.L. *Proc. Natn.Acad Sci.* (1955) **41** 629